VICTORIA UNIVERSITY
MELBOURNE AUSTRALIA

In situ small angle X-ray scattering investigation of the thermal expansion and related structural information of carbon nanotube composites

This is the Accepted version of the following publication

In situ small angle X-ray scattering investigation of the thermal expansion and related structural information of carbon nanotube composites

Authors

Ludovic Dumée[1,6*], Aaron Thornton[2], Kallista Sears[2], Jürg Schütz[2], Niall Finn[2], Steven Spoljaric[3], Robert Shanks[4], Chris Skourtis[1], Mikel Duke[5], Stephen Gray[6]

1 Institute for Frontier Materials, Deakin University, Pigdons Road - Waurn Ponds campus, Geelong, Victoria 3216 – AUSTRALIA

2 CSIRO Materials Science and Engineering, Clayton, Victoria 3108 – AUSTRALIA

3 Department of Biotechnology and Chemical Technology, Aalto University School of Chemical Technology, Aalto, Espoo, FINLAND

4 School of Applied Sciences, RMIT University, La Trobe St, Melbourne, Victoria 3000, AUSTRALIA

5 School of Engineering and Science, Victoria University, Hoppers Crossing, Victoria 3029 – AUSTRALIA

6 Institute for Sustainability and Innovation, Victoria University, Hoppers Crossing, Victoria 3029 – AUSTRALIA

*Corresponding author: ludovic.dumee@deakin.edu.au; +61410131312

1. Introduction

Carbon nanotubes (CNTs) have shown great promise towards solving some of the major challenges in materials science for sustainable and environmental applications [1-3]. A better understanding of CNT structures dynamic properties, such as thermal, electrical or mechanical, are desperately required to further expand their scope of application [4, 5]. Despite the fact that most of CNT nano-composite properties rely on the intrinsic and well defined CNT features, such as their length, diameter [6] or functional groups within the CNT graphene crystalline walls [7], some of the composite properties currently remain un-optimised due to the lack of experimental techniques to clearly understand interactions between CNTs and the surrounding matrix [8].

CNTs have, for instance, been incorporated into a number of nano-devices and nano-structures [2], such as flexible circuits in order to form a continuous network conducting current with their naturally high electrical conductivity [9, 10] or as promising base material for electrodes for fuel cells [11-13]. CNTs assemblies were also used to spin yarns [4] and sheets, used in the preparation of electronic circuits [4, 14] or as strain sensors [15]. In addition, CNTs used as nano-fluids and additives in solvents were also shown to increase the bulk fluid thermal and electrical characteristics [16] resulting in highly promising liquids for refrigeration and heat management [17, 18]. Research on plain and porous nano-composite materials has also demonstrated that the addition of low amounts of CNTs could also enhance the mechanical properties of the matrix [19-21]. CNT arrays, used as membrane pores, were demonstrated to exhibit superior performance due to their smooth friction-less surface potentially improving the permeation by a few decades over current commercial membranes [1, 22, 23]. Issues related to CNT aggregation when suspended in solution still generate hundreds of publications every year [24-26] while the control of the CNT orientation within mixed matrix composites remains challenging [27-29], limiting the ability to fully benefit from the CNTs natural properties.

Thermal properties of CNT based materials are critical for many applications, as they will typically dictate the boundary conditions within which any material can be handled and processed, and may define the scope of their final applications [30, 31].

Despite encouraging predicted values of CNT thermal properties, these remain to date the least investigated of their properties [32, 33]. The thermal properties of CNT arrays and CNT composites are especially difficult to obtain for a number of reasons. Large variations of the reported CNT thermal conductivity, diffusivity or expansion coefficients can be attributed to the limitations of some of the experimental procedures and discrepancies due to sample preparation or CNT purity, therefore making any scale-up of CNT for thermal property application difficult [3, 34, 35]. The determination of the thermal conductivity, typically performed with direct contact techniques, is for instance greatly affected by the difficulty to correctly evaluate the true area of contact between the probe and the sample, due to the high specific area, mechanical compressibility and porosity of most nano-structured materials [21]. On the other hand, thermal diffusivity, previously obtained with non-contact procedures such as the laser flash technique [36-38], has proven to be a more reliable way to determine the thermal properties of nano-structured materials [39]. Furthermore, although several studies have focused on the measurement of the thermal expansion of CNT polymer composites [40] and individual CNTs [41], little work has been performed on self-supporting CNT structures such as arrays [42], bucky-papers (BPs) or forests. Most of the techniques used to date to evaluate their thermal expansion have also relied on direct-contact methods that can be unreliable due to difficulty to controlling the interface between the sample and the probe used to quantify dimensional changes. Better methods to accurately and reproducibly obtain CNT array and composite thermal expansion coefficients are therefore desperately needed to provide better understanding of the phonon diffusion within CNT arrays and both CNT/CNT and CNT/matrix interactions when subjected to a thermal gradient.

This work reports for the first time the determination of the thermal expansion of a number of self-supporting and composite CNT materials with a non-contact technique. CNT composites, consisting of self-supporting, acetone densified, metal plated and polymer infiltrated BPs, as well as a reference polymer embedded CNT forest, were tested over a range of different temperatures. In order to avoid the drawbacks of the previously mentioned procedures, thermal expansion data were obtained by analysing Small Angle X-ray Scattering (SAXS) patterns of samples at

thermal equilibrium with a highly coherent and bright X-ray source at the Australian Synchrotron (AS).

X-rays diffraction typically probes electronic density fluctuations within a matrix and scattering of X-ray occurs from the scattering contrast difference between the various components that make up the material, typically reflecting density or structural changes within a given structure. During SAXS experiments, a beam of fixed wavelength and known intensity X-rays is set normal to the sample surface to probe. Although the main beam is stopped after crossing the sample, the intensity of the scattered radiation generated by small angle scattering across the sample can be recorded. Although SAXS measurements are technically challenging because of the small angular separation between the main X-ray beam and the scattered beam array, large sample-to-detector distances in the range of a few meters coupled with both high quality collimating optics, used to reduce signal to noise ratio, and very bright and monochromatic X-ray sources, such as a Synchrotron, can provide very good signal quality. Information relative to the size distribution of scattering objects or of the space between these nano-objects can be retrieved from the scattering intensity plotted versus the scattering vector:

$$q = \frac{4\pi}{\lambda} \sin(\frac{\theta}{2})$$

(1)

Where q is the scattering vector forming a scattering angle theta with the beam direction and lambda is the beam wavelength.

In fact, SAXS measurements are typically concerned with scattering angles smaller than 1° and therefore allow for probing dimensional structures from a few nano-metres up to a few thousand nano-metres depending on the experimental set-up and the camera length used [43, 44]. As dictated by Bragg's Law [44], the diffraction information of large nano-structures, is determined by the inter atomic plane distances, typically referred to as d-spacing. Angles in this region can potentially correspond to macro-molecules, high molecular weight polymers, large self-assembled superstructures or nano-particle assemblies within this region. SAXS experiments have proven particularly useful in porous materials characterization providing critical information about pore connectivity [45], pore alignment or density

[46], as well as allowing for direct qualitative characterization of dynamic systems [47], such as nano-particle aggregation and formation [48].

In this work, several specific features could be detected, including the CNT/CNT distance, the space between the CNT walls [49], or the type of CNT distribution (anisotropic [50], aligned in a plane normal to the beam, twisted around an axis or parallel tubes in line with the beam [51, 52]). These qualitative SAXS trends, investigating the interactions between CNTs within a small nano-scale window will be discussed and compared with thermal expansion results obtained from thermo-mechanical analysis, where the macroscopic mechanical properties were recorded at different temperatures.

2. Materials and method

2.1 Samples preparation and characterization

Self-supporting BPs were processed from chemical vapour deposition grown multi-walled CNTs as described in a previous study [53]. The CNTs were scraped from their silicon wafer growth substrates and dispersed in propan-2-ol by 5 repeated cycles of freezing at −17 °C followed by bath sonication using a method reported previously in [54]. The CNT suspension was then filtered on top of a porous 0.2 μm pore size poly(ether sulfone) (SHF – Merck-Millipore) membrane to form a self-supporting BP. In order to test the impact of solvent evaporation on the CNT network [55], self-supporting BPs were immersed in acetone and allowed to dry for 24 h in air and at room temperature. BPs were infiltrated by a 5 wt% poly(styrene) (PS) dimethyl-formamide (DMF) solution with a house line vacuum system. Gold plated BPs were processed by first exposing the self-supporting un-plated BP for 10 min to a flow of UV induced ozone in order to form hydroxyl groups at the surface of outer CNT walls. These groups are needed to facilitate wetting of the CNTs by the plating solutions and as anchors for the initial plating reactions. Then, the procedure for electroless gold deposition described by Martin et al. in [11] and previously used to fabricate pure gold nanotubes [56] and gold plated CNTs [57] was followed. Plating time was fixed at 20 h, in order to allow for reduction of the gold cations onto the negatively charged hydroxyl sites on the CNTs and to grow pure gold particles of a few nanometres in dimension. As a reference for the CNT scattering patterns, as grown CNTs forests were embedded into poly(dimethyl-siloxane) (PDMS) and tested without further treatments.

Every sample was stored in an oven at 60°C prior to SAXS analysis in order to avoid water uptake. All chemicals used in this work were of analytical grade. The porosity of the samples was evaluated using perm-porosimetry with a He pyknometer Accu PYC II 1340 from Micromeritics while the specific surface area of the samples was obtained via BET using N_2 adsorption [57]. The thickness of the samples were estimated with Scanning Electron Microscopy (SEM) image analysis and with a Kincrome micrometer [54]. Other references to experimental procedures can be found in the references in

Table **1**.

2.2 SAXS experiments

The SAXS beam-line at the Australian Synchrotron was used with a 1.6 m camera length to investigate the scattering patterns of the BPs within a 0.015 to 0.095 $Å^{-1}$ q range. The end-station uses a 1M Pilatus detector for SAXS and a 200k Pilatus detector for WAXS (wide angle detection) that provides excellent dynamic range, single photon per pixel sensitivity, low noise and fast time resolution (30 and 150 frames per second respectively). An In-vacuum undulator source, (22 mm period, 3 m length maximum, K_{max} 1.56) with an energy range between 5 and 21 keV was used. Energy beam values were maintained constant during all the measurements at 8.15 keV (resolution of 10^{-4} from a cryo-cooled Si(111) double crystal monochromators). The beam size at the sample was 250 µm horizontal × 150 µm vertical. The samples were heated within the SAXS chamber with a Linkam Scientific HFSX350 heating stage fitted with a THMS600 heating block. The stage was also fitted with a water cooled jacket in order to keep the stage body cool. The temperature of the stage was data-logged and the heating and cooling rates were fixed at 50 and 30 K/min respectively. A thermocouple was placed on the heating stage and the accuracy of the temperature measurement was estimated to be close to $0.1^{o}C$. Tests were performed at 50, 100, 150, 200, 300 and $400^{o}C$. Scattering patterns were acquired at each temperature plateau after stabilization for at least 1 min.

2.3 Modulated temperature – thermo-mechanometry

Modulated temperature – thermo mechanometry (mt-Tm) is a novel technique to determine reversing and non-reversing specimen changes under the application of an oscillating temperature to a linear/isothermal underlying heating rate [58]. A sinusoidal response is induced by the modulated temperature program that can be resolved into reversing (in phase with dT) or non-reversing (out-of-phase with dT) components. A TA Instruments Q400EM thermo-mechanical analyser was used to study the thermal expansion of the self-supporting BP samples. Samples with a

height of 100 μm were heated from 50°C to 250°C at a rate of 0.5°C.min^{-1}. A sinusoidal modulation with 2°C amplitude and 180 s period was superimposed to the temperature ramp. Every sample was heated up to 250°C for 5 min prior to the test in order to eliminate the thermal history of the material. The linear thermal expansion coefficient, α, was calculated from Equation 2:

$$\alpha = \frac{1}{dT} \cdot \frac{dL}{L_0}$$

(2)

Where dL is the change in length, dT the change in temperature and L_0 the initial length of the sample.

3. Results and discussion

A series of 5 independent samples were tested for their thermal expansion properties. CNTs exhibited very good thermal stability with a maximum mass loss at $400^{o}C$ of only ~3.5% (TGA results presented in [59]). Part of this loss was attributed to water, volatile organics and from the combined desorption and evaporation of solvent present on the CNTs. In addition, as the self-supporting BPs made of these multi-walled CNTs exhibited very large porosity (~90%), they offered an interesting platform for the fabrication of porous composite materials, such as the PS or gold plated BPs presented in this study. Furthermore, although solvent evaporation from a CNT array was previously shown to lead to the densification of the CNT structure [60], no proof of the stability of the densified structure was to date demonstrated. Despite an increase in mechanical strength and slight decrease of inner porosity, the structure of acetone densified yarns was found to be similar to that of non densified yarns [55]. For this reason the acetone densified self-supporting BPs should exhibit similar structure to non-densified yarns. The purity of the raw material, evaluated by thermo-gravimetric analysis, was very high as previously demonstrated in a number of our studies, therefore limiting the risk for contaminants to alter the SAXS scattering patterns [57, 59, 61]. All relevant properties of these materials are listed in

Table **1** for reference.

Table 1 Samples properties and preparation procedures

Sample	Nature	Treatment	Thickness	Porosity	Specific surface area	Mass loss at 400°C	Ref.
			µm	%	m^2.g^{-1}	%nominal	
Self-supporting	CNT BP	None	4	90	197	2	[59]
Acetone densified	CNT BP non woven	Dipped in acetone and dried	4	<90[+]	[+]	[+]	[1]
PS infiltrated	BP infiltrated with PS	Infiltrated with a 5wt% solution	25	65	95	[*]	[62]
Gold plated	BP coated with gold (90 wt% gold in mass)	Electroless deposition for 20 h	25	42	37	3.5	[57]
Reference CNT forest	Forest used to prepare the BP	Embedded in PDMS for stability	~100	N/A [$]	N/A	~2	[55]

[+]lower or similar to self-supporting BP

[*] PS melts at 240°C but degrades above 420°C

[$] The CNT surface density was estimated to be close to 10^{10} CNT.cm^{-2} from SEM analysis corresponding to ~98 % porosity

Figure 1 shows the diffraction patterns at 50°C and SEMs of the different structures while Figure 2 present their scattering intensity as a function of the scattering vector q. Due to the cooling of the stage between samples, the normalization of the "room temperature value" was rendered difficult and 50°C was therefore chosen as the reference temperature for the study as it allowed for consistent and systematic analysis of the different structures. For all the samples tested, and at any temperature investigated, the scattered intensity curves gradually decrease over the entire scattering vector range indicating the presence of a random distribution of scattering in-homogeneities (Figure 9 and Figure 10 – supplementary materials). The intensity curves obtained were analysed based on the Guinier

approach [43] . According to the Guinier formula the intensity of X-ray small angle scattering for mono-dispersed system is:

$$I(q) = I_0 . \exp(-\frac{1}{3}q^2 . R_g^2)$$

(3)

Where q is the scattering vector of a given inhomogeneity, I is the intensity of the scattering vector and R_g is the Guinier's electronic inertia radius of the in-homogeneity [43].

In addition, the difference of scattering intensity can also be attributed to the relative density of each sample, with typically, larger intensity correlating with lower porosity. The scattering intensity of the acetone densified BP exhibits stronger scattering intensity than the as-processed BP, indicating that it has lower porosity. This is in agreement with previous literature, where solvents are used to collapse (Figure 1) CNT arrays together to form denser structures. This process of densification is also demonstrated in Figure 3 where two CNT webs, drawn from similar spinnable forests [4] as the ones used in this study, were Gallium ion milled to reveal their inner porosity. The as-drawn CNT webs are highly porous with a thickness on the order of 20 um and are commonly densified to a thickness on the order of 100 nm [63]. The acetone densified sample (Figure 3 B and D) is clearly denser than the non-densified sample (Figure 3 A and C). The global scattering intensity for all the samples was found to decrease for the self-supporting BP with increasing temperatures as shown in Figure 9 (supplementary materials). The high precision of the SAXS is therefore a clear asset for this study as it allows the detection of nanometre changes in contrast to contact techniques previously described.

The scattering pattern (Figure 1 E) obtained for the PDMS embedded CNT forest, made of similar, but CNTs of slightly larger diameters, clearly shows an anisotropic structure with well distinguished rings. This structure is well supported by the corresponding SEM image of the forest showing CNT alignment. This sample was used to identify Guinier's knees on the BP composite scattering patterns similarly to that performed in [64, 65]. As seen in Figure 2, a shift around 10^{-2} Å^{-1} is

visible between the scattering patterns corresponding to the PDMS embedded forest and the other BP samples. The distance between two scattering features can be calculated at small scattering angles (less than 5°) following Equation 4:

$$d = \frac{2\pi}{q}$$

(4)

The iso-intensity lines visible at higher scattering angles on Figure 1 correspond to weaker scattered intensity which suggests a lower isotropicity of smaller features. These features, as seen in Figure 2, probably correspond to the distance between CNTs [66]. The CNT-CNT distance at 50°C is therefore found to lie around 5 nm which is in good agreement with the corresponding van der Waals radii modelled for CNTs within an entangled BP [67]. It is worth noting that the spaces between the graphene planar walls [68] were not visible on this q range window which covered a d-space range comprised between 7 and 400 Å (Equation 4) [69]. In addition, the presence of the small gold nano-particles (NPs), clearly visible on the micrograph in Figure 1D, can also be found from the broad scattering band between 2.10^{-3} and 2.10^{-2} A^{-1} of the gold plated sample in Figure 2. The broad scattering spectra of higher intensity can be attributed to the presence of a broad size distribution of gold NPs, and therefore makes difficult the precise determination of their size distribution. As shown in Table 2 (supplementary materials), there is relatively good consistency throughout the samples series between the corresponding spatial dimensions for the CNTs, while additional scattering peaks for the gold plated sample clearly indicate the presence of the NPs on the CNTs.

The position of the peak for the PDMS embedded forest is at a smaller q than that of the CNT BPs (Figure 2), meaning that the distance between the aligned CNTs composing the forest was therefore slightly larger than separation of CNTs within the BP samples. The fact that aligned CNTs are further apart within the forest indicates that the relative packing density of the forest is lower than that of the BPs. The density of CNT forest was previously estimated around 3×10^{10} CNT.cm^{-2} which corresponds to approximately 2.35 % of coverage in the case of 10 nm diameter CNTs [70]. This is clearly less dense than BP whose density was estimated from porosity measurements to lie around 8-10 % volume fraction [59].

All the BP samples, namely self-supporting (A), acetone densified (B), PS infiltrated (C) and gold plated (D) present an anisotropic SAXS pattern (Figure 1) suggesting a random distribution of particles across the sample with no preferential orientation [71]. For crystalline matter homogeneously composed of a single matrix phase, such as graphene in this study, the scattering of X-rays occurs simultaneously at the interface between the solid-void matrix of the pore space, and between the CNT graphene walls. The pattern of scattered intensity versus scattering angle is determined by the various length scales corresponding to the d-spaces between two close features. If the shape of individual pores is known or can be reasonably assumed, this scattering pattern can be modelled and translated into a pore size distribution [45]. In the present case, due to the complex interconnectivity of the pores, formed by the overlapping CNTs, and the anisotropy of the CNT distribution across the CNT BP, modelling the pore size distribution was not quantitatively performed.

As shown in Figure 4, a clear shift of peak positions was found to occur when temperature was increased from 50 to 400°C for the self-supporting BPs. Interestingly, this shift was not found on the acetone densified and PS infiltrated samples (Figure 5), suggesting that the structure in these later composites is set and that no further movement of CNTs can be achieved. This observation correlates well with the porosity trend shown in

Table **1** where porosity was found to be lower for these samples. The addition of PS into the structure consequently reduced the porosity by nearly 25%, clearly filling up part of the inner porosity. It is, however, surprising that no shift of the PS samples was found at temperatures exceeding the melting point of the PS (~240°C). This suggests, as seen on the SEM image in Figure 1-C, that the PS network is relatively homogeneous and that the melting of the polymer did not lead to high surface tension forces which could have been expected to draw the CNTs together following the melting of PS. It is also possible that the CNT network was already densified due to the evaporation of DMF used for the PS dissolution in a similar fashion as that of acetone densified samples. Further tests should be performed to properly understand this trend. However, the formation of 2 new permanent peaks above 300°C (for scattering vectors q of 0.0527 and 0.0534 respectively – see supplementary materials) suggests an overall structural modification supporting the theory of polymer melting effect over that of solvent densification, as no solvent should be left within the sample at this stage of the test.

In addition the gold plated sample also exhibited both peak shifts and disappearances (supplementary materials) suggesting that NP sintering occurred during the process. The reactivity of gold NPs [57, 72, 73] is known to be high and the exposure to strong X-ray energies could have effectively forced some closely packed particles to fuse into more stable larger particles or rearrange into a different particle distribution. The non-monotonic regime of this shift (Figure 5) seems to indicate that multiple effects are simultaneously affecting the morphology of the sample. It was for instance shown by Ristau et al. [73] that the NP size, temperature of aggregation and concentration were affecting the aggregation or splitting mechanisms. Unlike that work [73], the large size of the NPs present on the CNTs in our work (close to 50-80 nm in diameter) could lead to a split of the NPs into smaller aggregates as described in [74]. The SAXS tests performed for these samples do not, however, allow a conclusion to be reached on the large scale thermal expansion of the structures due to a camera length of only 1.6 m. The scattering of larger patterns, such as CNT macro-aggregates of a few dozen nano-meters or more would need a longer camera length to gather x-rays generated from such small angle scattering. This should be performed in order to generalize the trends obtained at the level of CNT bundles and small agglomerates.

According to the definitions of the Guinier radius, R_G [43, 49], as the temperature increases, the scatter from the small scale features reduce in number while their size decreases. It is likely that in this case, due to the increased temperature and the natural large porosity of the BPs, CNTs tend to aggregate within the BP, thus densifying the structure. The Q-range window, corresponding to the total X-ray invariant, chosen for these tests was found afterwards to be slightly too low (shift towards small features) to be conclusive. The window covered a range from 0.44 to 40 nm, which was initially thought to be sufficient to cover the range where CNT would agglomerate and form denser or looser bundles. Therefore, the global behaviour on a macro-scale was found difficult to interpret and more SAXS tests at higher Q would be required to fully comprehend the BP behaviour. Work by Zhao et al. on the bundling kinetics and bundle formation showed that bundles may spread over a larger range [49]. In that work, the samples were exposed to different acid treatments to provide information on their dispersion state. At CNT bundle sizes smaller than 100-300 nm, all their samples behaved identically. However, after 24 h of treatment their SAXS patterns undertook a flip at q-ranges values corresponding to ~300 nm features. This was attributed to a change in the bundle morphology that they described as precipitation, or aggregation, of the tubes. Their dispersion method seemed to have a clear effect at longer treatment times increasing intensity, which was attributed to looser bundle formation improving the dispersion of CNTs [49].

The Luh graph [43] (Figure 6) amplifies the structural feature over time. First, it is visible that the structural features decrease in steps until 400°C, corresponding to the maximum tested temperature. However, at the end of the cooling period, and return to the 50 ºC benchmark, a permanent change of relative intensity, noted by h on the graph, can be seen. This is an important feature as it shows that the BP are thermally stable but can endure permanent deformation due to thermal stress at high temperatures (above 200 – 250 ºC). This permanent deformation correlates well with the mt-Tm tests, which demonstrated that an important part of the deformation was permanent and non-reversible at high temperatures (above 300 ºC) [49]. This test, performed on a 100 µm thick BP was performed to assess the thermal expansion of the BP structure on a macro-scale (Figure 8-A). Interestingly, the irreversible contribution was found to be negative and larger than the reversible contribution, indicating a sharp contraction of the structure (Figure 8-B). As the graphene walls of

CNTs were previously demonstrated to expand with temperature [75], this macro-change is therefore attributed to the collapse of the BP structure and not to changes of the lattice of individual CNTs. Through computational modelling of their high thermal diffusivity and conductivity were computed [76, 77] and single walled CNTs were predicted to exhibit thermal conductivity up to 10 kW/m×K [78] along their axis, which is 3 times greater than diamond, one of the best conducting material known [79], while multi-walled CNTs were assumed to go up to ~3 kW/m×K [80]. In addition, it is interesting to note that this discrepancy occurred despite pre-test heat treatment of the sample in order to remove any thermal history. Due to this reasonably high pre-treatment temperature, the permanency of the deformation is therefore questionable. In fact, the discrepancy of the signal on the Luh graph could be explained by a relatively long relaxation time of the material. This relaxation state would require higher temperatures to be fulfilled and could have therefore been detected with the SAXS at temperatures higher than $250^{o}C$. This anomaly could therefore be related to remaining mechanical strains across the sample, induced during fabrication. The deformation could then be either semi-permanent, the sample relaxing back slowly over long time scales, or permanent, if the material allows for further deformation, i.e. by more than it did in the pre-relaxing step, under the thermal strain of the test. This interesting result does however require further investigation in order to be solved.

A number of studies previously investigated heat transfers across individual or arrays made of CNTs. CNTs can be considered 1-D electron conductors because of their very high aspect ratio. The thermal conductivity and expansion of materials as governed by phonon diffusion and scattering within complex CNT structures such as BPs can be affected by a number of factors including the CNTs chirality and the amount of impurities and functional groups present on the CNT walls structure [81]. Thermal expansion of small single walled nanotubes bundles was shown to be close to that of graphite lattice and reported values lay between 2 and 4.2 $\times 10^{-5}$ K^{-1} [42, 82]. Studies on the behaviour of CNT/polymer extruded filaments or cast films composite materials showed an important increase in the axial thermal expansion. Those enhancements were attributed to lattice vibrations between carbon atoms [83]. On the other hand, the present authors previously presented [84] thermal expansion results on the same type of BP structure performed within an

Environmental SEM at temperatures between 50 and 400°C. In this work performed in a low pressure nitrogen atmosphere, the self-supporting BPs were also demonstrated to undertake thermal contraction under thermal gradient. A technical difficulty with this technique was shown to be related to the accuracy of the measurement of the sample thickness. Very small changes visible on the SEM micrographs could not be definitely attributed to true dimensional changes as a number of factors, including drift of the mounting stage due to the thermal gradient, contact between the sample and the holder as well as expansion of the copper holder, could clearly affect the readings. Although the self-supporting BP structure was 100 microns thick, changes of the order of 0.1 microns were difficult to detect due to the inability to simultaneously image at high (CNT scale) and low resolution (BP scale). Very little has been published on the thermal expansion of pure macro structures made of multi-walled CNTs and more research is therefore required to fully comprehend the phonon diffusion mechanisms and the impact of large thermal gradients on macro-structures made of CNTs.

Despite the fact that no thermal expansion coefficients were calculated from this experiment, the SAXS measurements clearly showed that CNT BP were physically affected by large temperature variations and that thermal ageing such as permanent or semipermanent deformation was to be expected above 200 °C. As shown in Figure 7, the radius of gyration and the Guinier scattering radius did change as a function of temperature. A significant decrease in the gyration radius is visible above 250 °C, corresponding to the formation of larger features [43, 49]. A possible explanation of the origin of this thermal contraction could reside in the fundamentals of the CNT/CNT interactions. CNT self-assemblies have been shown to be held together by van-der-Waals forces only, which are affected by temperature, as previously demonstrated for colloid and agglomerate formation in liquids [49]. The Van der Waals forces may help attract the CNTs together, thus overwhelming the individual CNT thermal expansion to form denser structures up to a maximum bundling density. This might explain the negative thermal expansion, corresponding physically to a thermal contraction but further experiments and research is required to assess this theory.

4. Conclusions

Investigations of 5 different CNT composites were performed in order to evaluate the impact of temperature on their thermal expansion with a non-contact method based on SAXS. Although this qualitative new method offers interesting perspective for the analysis of the thermal properties of nano-materials, the main limitation at this stage remains in benchmarking the results with a specific material in order to obtain quantitative trends. This should be investigated as it would open a new era to the characterisation of materials for sustainable development. The present results indicate that solvent densification leads to more thermally stable structures and that considerable contraction can occur within CNT BP structures when undertaking thermal stress. Although these preliminary results give guidelines for medium to high temperature applications for self-supported CNT structures, it was also demonstrated that polymer reinforcement prevented this thermal contraction.
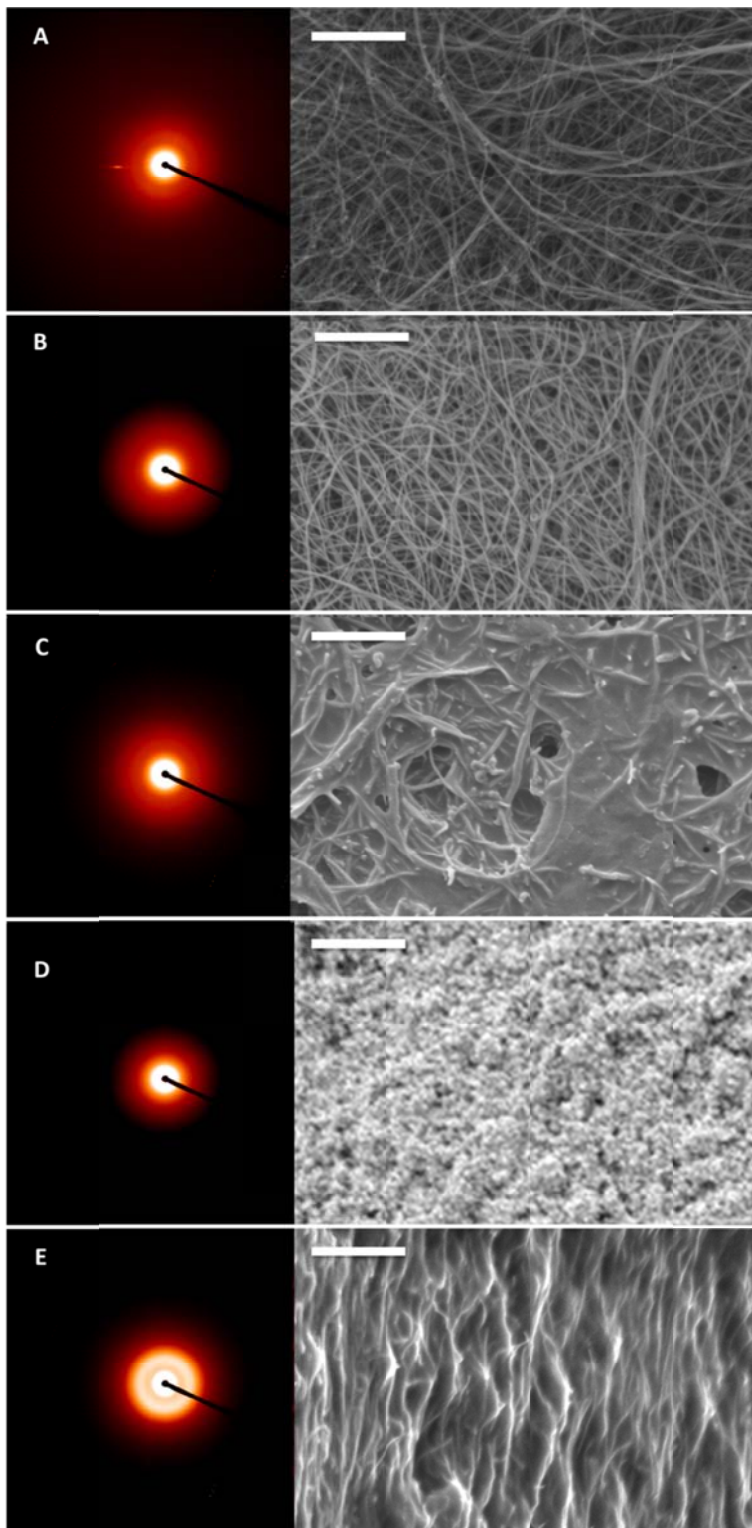
Figures

Figure 1 SAXS patterns at 50°C (left) and corresponding SEM image (right) of (A) self-supporting BP; (B) acetone condensed BP; (C) PS infiltrated BP; (D) 20h gold plated BP; and (E) reference CNT forest; the scale bar on the top image correponds to 1 μm and is the same for all the images
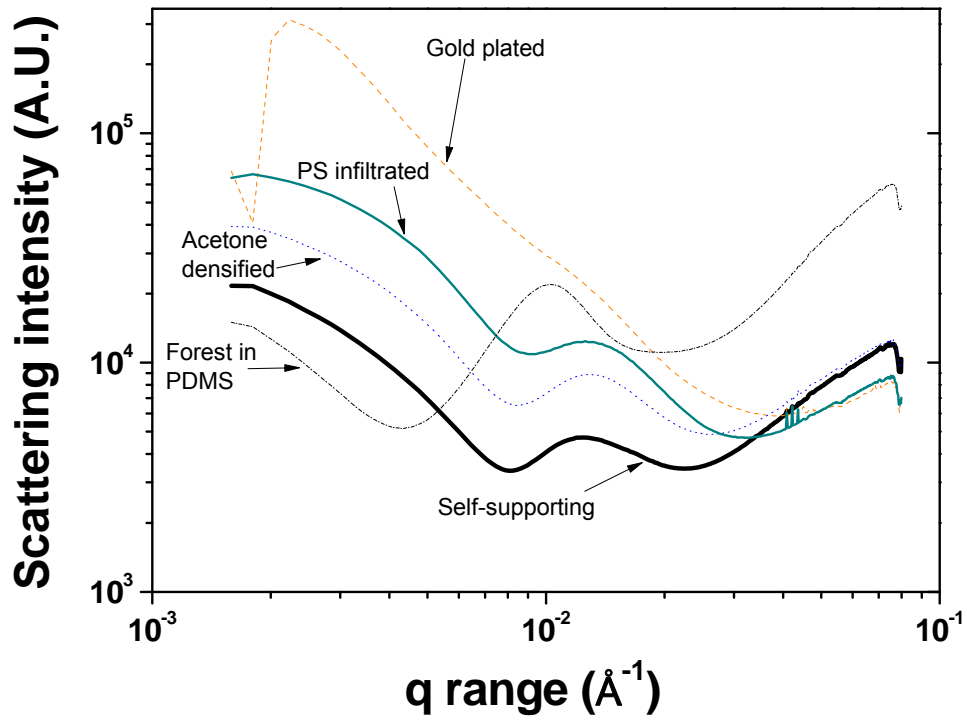
Figure 2 Typical scattering intensity as a function of the scattering vector q for the 5 different samples at $50^{o}C$
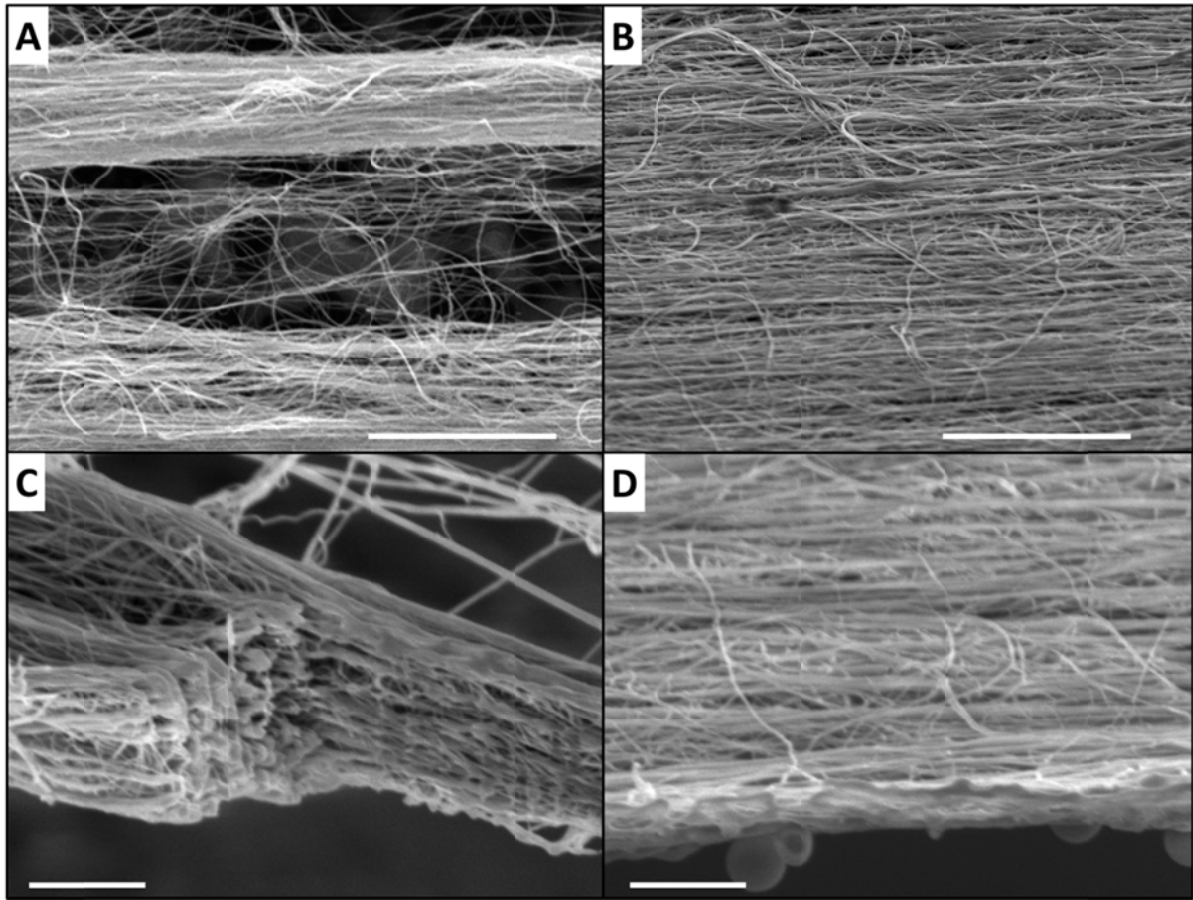
Figure 3 SEM images of 10 layer webs as drawn (left) and acetone densified (right); A and B correspond to the surface view of the webs (scale bar is 4 µm for both images); while C and D correspond to Focus Ion Beam (FIB) cross sections (scale bar is 1 µm for both images)
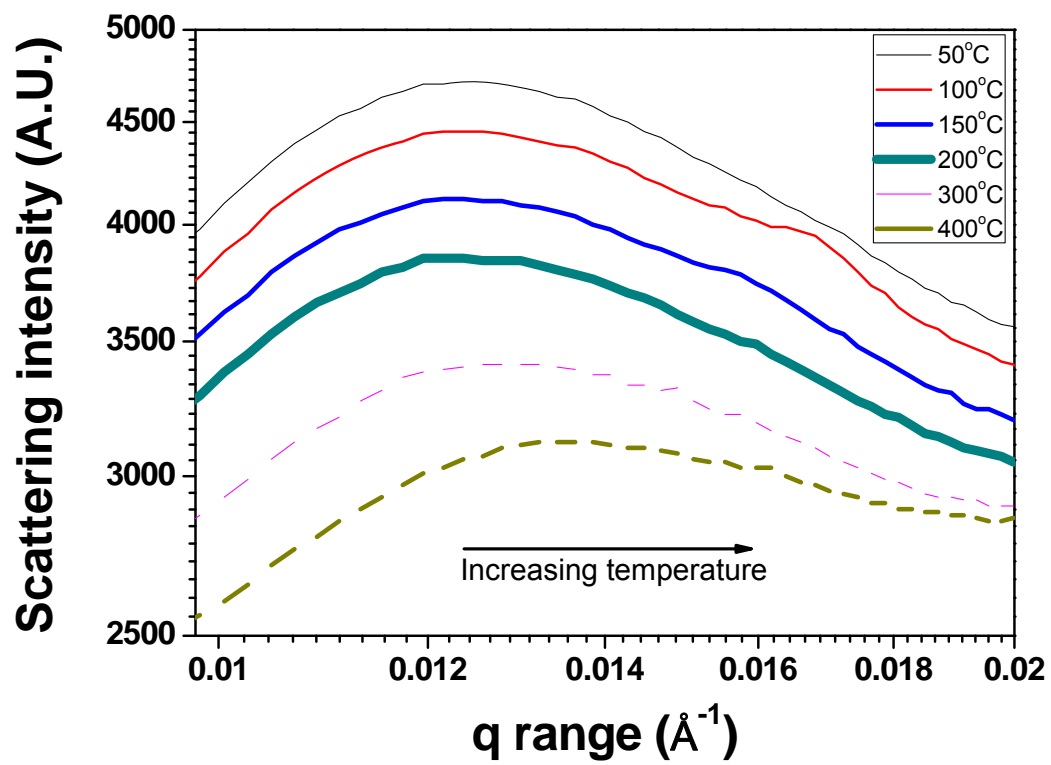
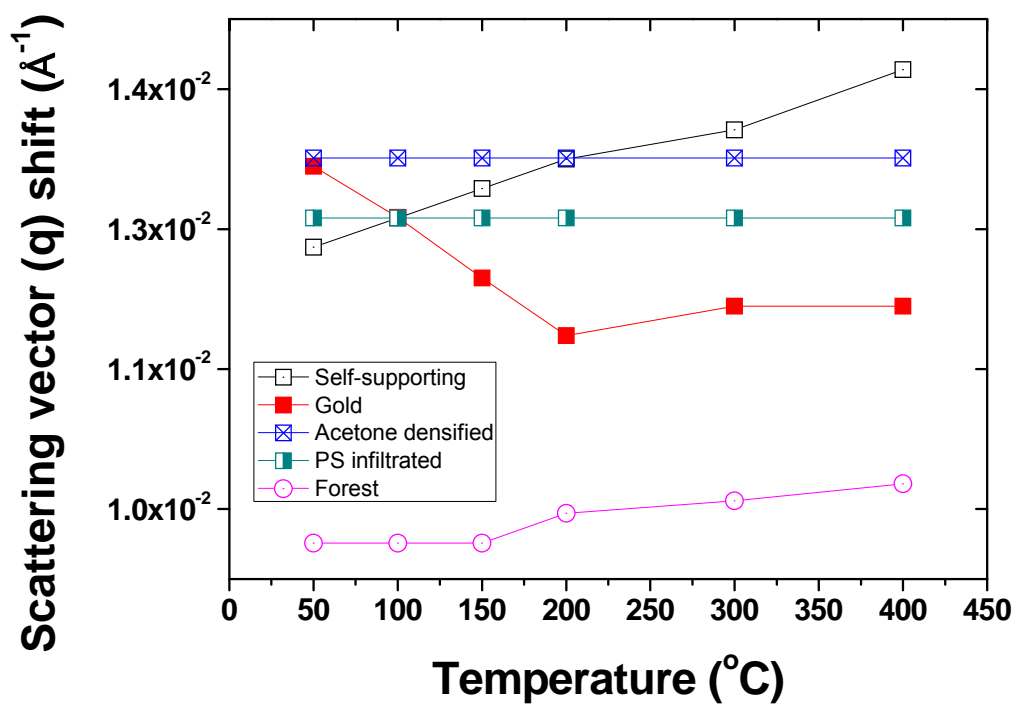Figure 4 Self-supporting BP peak shift with temperature

Figure 5 Shift of the 1st peak – acetone densified and PS infiltrated samples were found to be constant
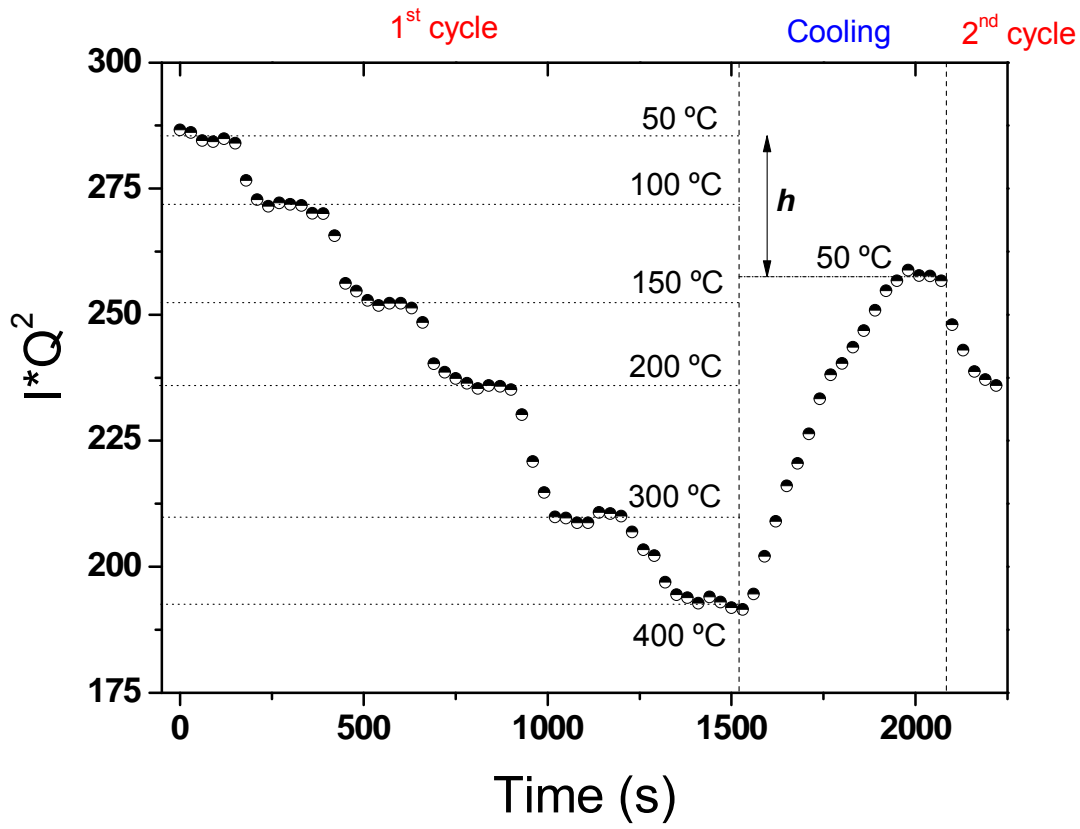
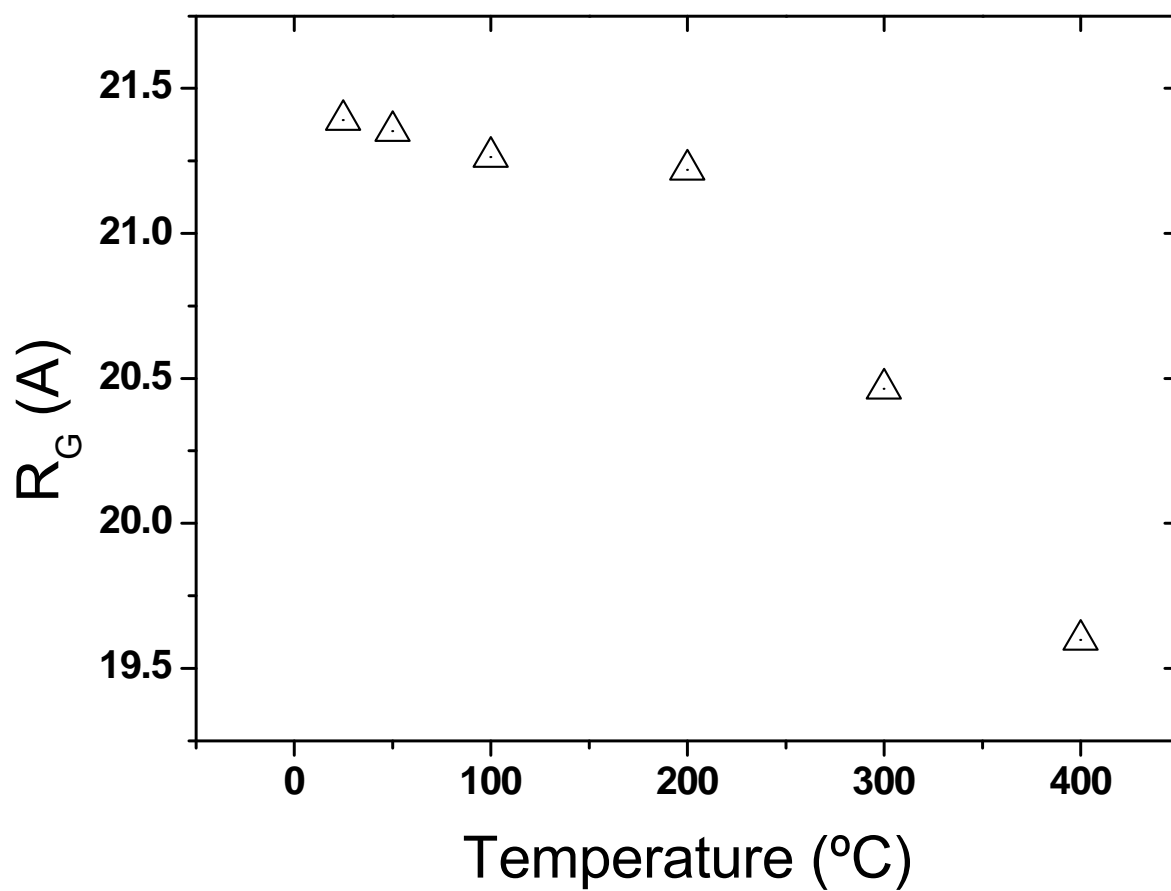Figure 6 Luh graph for the self-supporting BP

Figure 7 Radius of gyration as a function of temperature for a BP self-supporting sample
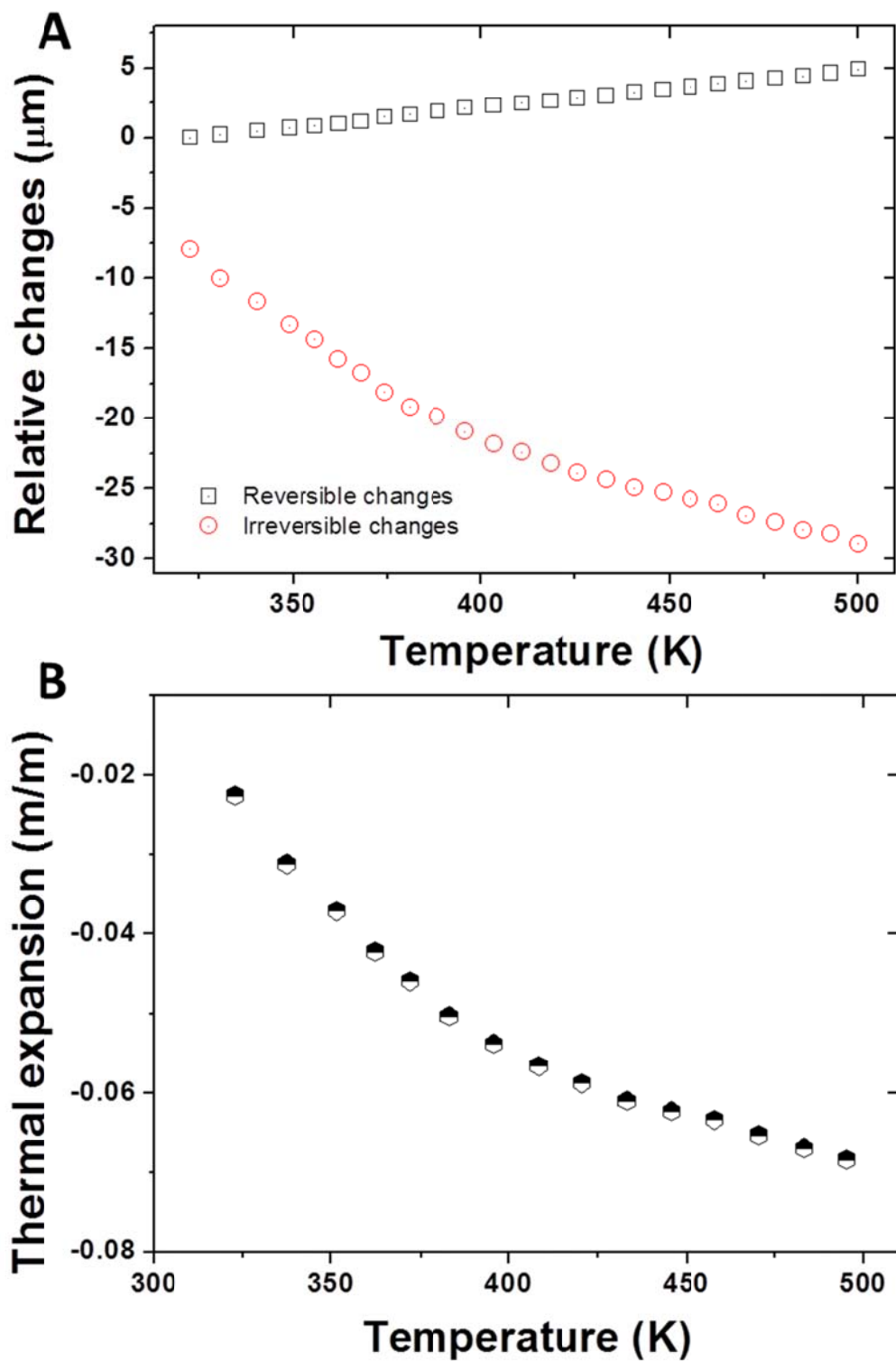
Figure 8 A) mT-Tm of a self-supporting BP showing reversible and irreversible contraction; B) Overall thermal expansion coefficient with the mt-Tm method

References

[1] Sears K, Dumee L, Schuetz J, She M, Huynh C, Hawkins S, et al. Recent Developments in Carbon Nanotube Membranes for Water Purification and Gas Separation. Materials. 2010,3 (1):127-49.

[2] Martinez-Hernandez AL, Velasco-Santos C, Castano VM. Carbon Nanotubes Composites: Processing, Grafting and Mechanical and Thermal Properties. Current Nanoscience. 2010,6 (1):12-39.

[3] Prakash S, Kulamarva AG. Recent advances in drug delivery: potential and limitations of carbon nanotubes. Recent patents on drug delivery & formulation. 2007,1 (3):214-21.

[4] Atkinson KR, Hawkins SC, Huynh C, Skourtis C, Dai J, Zhang M, et al. Multifunctional carbon nanotube yarns and transparent sheets: Fabrication, properties, and applications. Physica B: Condensed Matter. 2007,394 (2):339-43.

[5] Endo M, Strano MS, Ajayan PM. Potential applications of carbon nanotubes. Carbon nanotubes advanced topics in the synthesis, structure, properties and applications. 2008:13-61.

[6] Majumder M, Chopra N, Andrews R, Hinds BJ. Nanoscale hydrodynamics: Enhanced flow in carbon nanotubes. Nature. 2005,438 (7064):44-.

[7] Zhou J, Wang C, Qian Z, Chen C, Ma J, Du G, et al. Highly efficient fluorescent multi-walled carbon nanotubes functionalized with diamines and amides. Journal of Materials Chemistry. 2012,22 (24):11912-4.

[8] Buldum A, Lu JP. Contact resistance between carbon nanotubes. Physical Review B. 2001,63 (16):161403.

[9] Sun D-m, Timmermans MY, Tian Y, Nasibulin AG, Kauppinen EI, Kishimoto S, et al. Flexible high-performance carbon nanotube integrated circuits. Nat Nano. 2011,6 (3):156-61.

[10] Shi J, Guo CX, Chan-Park MB, Li CM. All-Printed Carbon Nanotube finFETs on Plastic Substrates for High-Performance Flexible Electronics. Advanced Materials. 2012,24 (3):358-61.

[11] Menon VP, Martin CR. Fabrication and Evaluation of Nanoelectrode Ensembles. Analytical Chemistry. 1995,67 (13):1920-8.

[12] Wang HM, Wu ZC, Plaseied A, Jenkins P, Simpson L, Engtrakul C, et al. Carbon nanotube modified air-cathodes for electricity production in microbial fuel cells. Journal of Power Sources. 2011,196 (18):7465-9.

[13] Jeng KT, Hsu NY, Chien CC. Synthesis and evaluation of carbon nanotube-supported RuSe catalyst for direct methanol fuel cell cathode. International Journal of Hydrogen Energy. 2011,36 (6):3997-4006.

[14] Lee RS, Kim HJ, Fischer JE, Lefebvre J, Radosavljević M, Hone J, et al. Transport properties of a potassium-doped single-wall carbon nanotube rope. Physical Review B - Condensed Matter and Materials Physics. 2000,61 (7):4526-9.

[15] Zhao H, Zhang Y, Bradford PD, Zhou Q, Jia Q, Yuan F-G, et al. Carbon nanotube yarn strain sensors. Nanotechnology. 2010,21 (30):305502.

[16] Xue HS, Fan JR, Hong RH, Hu YC. Characteristic boiling curve of carbon nanotube nanofluid as determined by the transient calorimeter technique. Applied Physics Letters. 2007,90 (18):184107.

[17] Zhang J-X, Zheng Y-P, Lan L, Mo S, Yu P-Y, Shi W, et al. Direct Synthesis of Solvent-Free Multiwall Carbon Nanotubes/Silica Nonionic Nanofluid Hybrid Material. ACS Nano. 2009,3 (8):2185-90.

[18] Harish S, Ishikawa K, Einarsson E, Aikawa S, Chiashi S, Shiomi J, et al. Enhanced thermal conductivity of ethylene glycol with single-walled carbon nanotube inclusions. International Journal of Heat and Mass Transfer. 2012,55 (13–14):3885-90.

[19] Ma W, Liu L, Zhang Z, Yang R, Liu G, Zhang T, et al. High-Strength Composite Fibers: Realizing True Potential of Carbon Nanotubes in Polymer Matrix through Continuous Reticulate Architecture and Molecular Level Couplings. Nano Letters. 2009,9 (8):2855-61.

[20] Dumee L, Sears K, Schuetz J, Finn N, Duke M, Gray S. A Preliminary Study on the Effect of Macro Cavities Formation on Properties of Carbon Nanotube Bucky-Paper Composites. Materials. 2011,4 (3):553-61.

[21] Han Z, Fina A. Thermal conductivity of carbon nanotubes and their polymer nanocomposites: A review. Progress in Polymer Science. 2011,36 (7):914-44.

[22] Hinds BJ, Chopra N, Rantell T, Andrews R, Gavalas V, Bachas LG. Aligned Multiwalled Carbon Nanotube Membranes. Science. 2004,303 (5654):62-5.

[23] Holt JK, Park HG, Wang Y, Stadermann M, Artyukhin AB, Grigoropoulos CP, et al. Fast Mass Transport Through Sub-2-Nanometer Carbon Nanotubes. Science. 2006,312 (5776):1034-7.

[24] Rastogi R, Kaushal R, Tripathi SK, Sharma AL, Kaur I, Bharadwaj LM. Comparative study of carbon nanotube dispersion using surfactants. Journal of Colloid and Interface Science. 2008,328 (2):421-8.

[25] Battisti A, Skordos AA, Partridge IK. Monitoring dispersion of carbon nanotubes in a thermosetting polyester resin. Composites Science and Technology. 2009,69 (10):1516-20.

[26] Vaisman L, Wagner HD, Marom G. The role of surfactants in dispersion of carbon nanotubes. Advances in Colloid and Interface Science. 2006,128–130 (0):37-46.

[27] Fan Z, Advani SG. Characterization of orientation state of carbon nanotubes in shear flow. Polymer. 2005,46 (14):5232-40.

[28] Seidel GD, Puydupin-Jamin AS. Analysis of clustering, interphase region, and orientation effects on the electrical conductivity of carbon nanotube–polymer nanocomposites via computational micromechanics. Mechanics of Materials. 2011,43 (12):755-74.

[29] Wood JR, Zhao Q, Wagner HD. Orientation of carbon nanotubes in polymers and its detection by Raman spectroscopy. Composites Part A: Applied Science and Manufacturing. 2001,32 (3–4):391-9.

[30] Rafii-Tabar H. Computational modelling of thermo-mechanical and transport properties of carbon nanotubes. Physics Reports. 2004,390 (4–5):235-452.

[31] Razeeb KM, Munari A, Dalton E, Punch J, Roy S, Asme. Thermal properties of carbon nanotube-polymer composites for thermal interface material applications. New York: Amer Soc Mechanical Engineers, 2007.

[32] Yang XS. Modelling heat transfer of carbon nanotubes. Modelling and Simulation in Materials Science and Engineering. 2005,13 (6):893-902.

[33] Hone J. Phonons and thermal properties of carbon nanotubes. Carbon Nanotubes. 2001,80:273-86.

[34] Lischner J, Arias TA. Material limitations of carbon-nanotube inertial balances: Possibility of intrinsic yoctogram mass resolution at room temperature. Physical Review B. 2010,81 (23):233409.

[35] Dumée LF, Gray S, Duke M, Sears K, Schütz J, Finn N. The role of membrane surface energy on direct contact membrane distillation performance. Desalination. 2012 (0).

[36] Ohta H, Shibata H, Suzuki A, Waseda Y. Novel laser flash technique to measure thermal effusivity of highly viscous liquids at high temperature. Review of Scientific Instruments. 2001,72 (3):1899-903.

[37] Nunes dos Santos W, Mummery P, Wallwork A. Thermal diffusivity of polymers by the laser flash technique. Polymer Testing. 2005,24 (5):628-34.

[38] Lin W, Shang J, Gu W, Wong CP. Parametric study of intrinsic thermal transport in vertically aligned multi-walled carbon nanotubes using a laser flash technique. Carbon. 2012,50 (4):1591-603.

[39] Xie H, Cai A, Wang X. Thermal diffusivity and conductivity of multiwalled carbon nanotube arrays. Physics Letters A. 2007,369 (1–2):120-3.

[40] Deng CF, Ma YX, Zhang P, Zhang XX, Wang DZ. Thermal expansion behaviors of aluminum composite reinforced with carbon nanotubes. Materials Letters. 2008,62 (15):2301-3.

[41] Ruoff RS, Lorents DC. Mechanical and thermal properties of carbon nanotubes. Carbon. 1995,33 (7):925-30.

[42] Pipes RB, Hubert P. Helical carbon nanotube arrays: thermal expansion. Composites Science and Technology. 2003,63 (11):1571-9.

[43] Beaucage G, Schaefer DW. Structural studies of complex systems using small-angle scattering: a unified Guinier/power-law approach. Journal of Non-Crystalline Solids. 1994,172-174 (Part 2):797-805.

[44] Guinier A, Fournet G, Walker CB, Yudowitch KL. Small-angle Scattering of X-rays. New York1955.

[45] Radlinski AP, Mastalerz M, Hinde AL, Hainbuchner M, Rauch H, Baron M, et al. Application of SAXS and SANS in evaluation of porosity, pore size distribution and surface area of coal. International Journal of Coal Geology. 2004,59 (3–4):245-71.

[46] Zhang J, Xie Z, Hill AJ, She FH, Thornton AW, Hoang M, et al. Structure retention in cross-linked poly(ethylene glycol) diacrylate hydrogel templated from a hexagonal lyotropic liquid crystal by controlling the surface tension. Soft Matter. 2012,8 (7):2087-94.

[47] Zhang F, Skoda MWA, Jacobs RMJ, Zorn S, Martin RA, Martin CM, et al. Gold Nanoparticles Decorated with Oligo(ethylene glycol) Thiols: Protein Resistance and Colloidal Stability†. The Journal of Physical Chemistry A. 2007,111 (49):12229-37.

[48] Fenniri H, Deng B-L, Ribbe AE, Hallenga K, Jacob J, Thiyagarajan P. Entropically driven self-assembly of multichannel rosette nanotubes. Proceedings of the National Academy of Sciences of the United States of America. 2002,99 (Suppl 2):6487-92.

[49] Zhao J, Schaefer DW, Shi D, Lian J, Brown J, Beaucage G, et al. How Does Surface Modification Aid in the Dispersion of Carbon Nanofibers? The Journal of Physical Chemistry B. 2005,109 (49):23351-7.

[50] Hernández JJ, García-Gutiérrez MC, Nogales A, Rueda DR, Ezquerra TA. Small-angle X-ray scattering of single-wall carbon nanotubes dispersed in molten poly(ethylene terephthalate). Composites Science and Technology. 2006,66 (15):2629-32.

[51] Wang BN, Bennett RD, Verploegen E, Hart AJ, Cohen RE. Characterizing the Morphologies of Mechanically Manipulated Multiwall Carbon Nanotube Films by Small-Angle X-ray Scatteringâ€ The Journal of Physical Chemistry C. 2007,111 (48):17933-40.

[52] Wang BN, Bennett RD, Verploegen E, Hart AJ, Cohen RE. Quantitative Characterization of the Morphology of Multiwall Carbon Nanotube Films by Small-Angle X-ray Scattering. The Journal of Physical Chemistry C. 2007,111 (16):5859-65.

[53] Dumee L, Campbell JL, Sears K, Schuetz J, Finn N, Duke M, et al. The impact of hydrophobic coating on the performance of carbon nanotube bucky-paper membranes in membrane distillation. Desalination. 2011,283:64-7.

[54] Dumee L, Germain V, Sears K, Schuetz J, Finn N, Duke M, et al. Enhanced durability and hydrophobicity of carbon nanotube bucky paper membranes in membrane distillation. Journal of Membrane Science. 2011,376 (1-2):241-6.

[55] Sears K, Skourtis C, Atkinson K, Finn N, Humphries W. Focused ion beam milling of carbon nanotube yarns to study the relationship between structure and strength. Carbon. 2010,48 (15):4450-6.

[56] Velleman L, Shapter JG, Losic D. Gold nanotube membranes functionalised with fluorinated thiols for selective molecular transport. Journal of Membrane Science. 2009,328 (1–2):121-6.

[57] Dumee L, Hill MR, Duke M, Velleman L, Sears K, Schutz J, et al. Activation of gold decorated carbon nanotube hybrids for targeted gas adsorption and enhanced catalytic oxidation. Journal of Materials Chemistry. 2012,22 (18):9374-8.

[58] Price DM. Modulated-temperature thermomechanical analysis. Thermochimica Acta. 2000,357–358 (0):23-9.

[59] Dumée LF, Sears K, Schütz J, Finn N, Huynh C, Hawkins S, et al. Characterization and evaluation of carbon nanotube Bucky-Paper membranes for direct contact membrane distillation. Journal of Membrane Science. 2010,351 (1–2):36-43.

[60] Liu Z, Bajwa N, Ci L, Lee SH, Kar S, Ajayan PM, et al. Densification of carbon nanotube bundles for interconnect application. New York: Ieee, 2007.

[61] Dumée LF, Sears K, Marmiroli B, Amenitsch H, Duan X, Lamb R, et al. A high volume and low damage route to hydroxyl functionalization of carbon nanotubes using hard X-ray lithography. Carbon. 2012 (0).

[62] Dumee L, Sears K, Schutz J, Finn N, Duke M, Gray S. Carbon nanotube based composite membranes for water desalination by membrane distillation. Desalination and Water Treatment. 2010,17 (1-3):72-9.

[63] Li C, Thostenson ET, Chou T-W. Sensors and actuators based on carbon nanotubes and their composites: A review. Composites Science and Technology. 2008,68 (6):1227-49.

[64] Prado LASdA, Kwiatkowska M, Funari SS, Roslaniec Z, Broza G, Schulte K. Studies on morphology and interphase of poly(butylene terephthalate)/carbon nanotubes nanocomposites. Polymer Engineering & Science. 2010,50 (8):1571-6.

[65] Jin L, Bower C, Zhou O. Alignment of carbon nanotubes in a polymer matrix by mechanical stretching. Applied Physics Letters. 1998,73 (9):1197-9.

[66] Das NC, Yang KK, Liu YY, Sokol PE, Wang ZG, Wang H. Quantitative Characterization of Vertically Aligned Multi-Walled Carbon Nanotube Arrays Using Small Angle X-Ray Scattering. Journal of Nanoscience and Nanotechnology. 2011,11 (6):4995-5000.

[67] Li Y, Kroger M. Viscoelasticity of carbon nanotube buckypaper: zipping-unzipping mechanism and entanglement effects. Soft Matter. 2012,8 (30):7822-30.

[68] Wang BN, Bennett RD, Verploegen E, Hart AJ, Cohen RE. Characterizing the morphologies of mechanically manipulated multiwall carbon nanotube films by small-angle X-ray scattering. Journal of Physical Chemistry C. 2007,111 (48):17933-40.

[69] Mudie S, Kirby N. SAXS Beamline Technical Specifications. 2008.

[70] Huynh CP, Hawkins SC. Understanding the synthesis of directly spinnable carbon nanotube forests. Carbon. 2010,48 (4):1105-15.

[71] Lemaire BJ, Panine P, Gabriel JCP, Davidson P. The measurement by SAXS of the nematic order parameter of laponite gels. EPL (Europhysics Letters). 2002,59 (1):55.

[72] Wu H, Bai F, Sun ZC, Haddad RE, Boye DM, Wang ZW, et al. Nanostructured Gold Architectures Formed through High Pressure-Driven Sintering of Spherical Nanoparticle Arrays. Journal of the American Chemical Society. 2010,132 (37):12826-8.

[73] Ristau R, Tiruvalam R, Clasen PL, Gorskowski EP, Harmer MP, Kiely CJ, et al. Electron microscopy studies of the thermal stability of gold nanoparticle arrays. Gold Bulletin. 2009,42 (2):133-43.

[74] Link S, El-Sayed MA. Size and Temperature Dependence of the Plasmon Absorption of Colloidal Gold Nanoparticles. The Journal of Physical Chemistry B. 1999,103 (21):4212-7.

[75] Pozzo M, Alfè D, Lacovig P, Hofmann P, Lizzit S, Baraldi A. Thermal Expansion of Supported and Freestanding Graphene: Lattice Constant versus Interatomic Distance. Physical Review Letters. 2011,106 (13):135501.

[76] Andreescu A, Savin A, Steigmann R, Iftimie N, Mamut E, Grimberg R. Model for thermal conductivity of composites with carbon nanotubes. Journal of Thermal Analysis and Calorimetry. 2008,94 (2):349-53.

[77] Mingo N, Broido DA. Length Dependence of Carbon Nanotube Thermal Conductivity and the "Problem of Long Waves". Nano Letters. 2005,5 (7):1221-5.

[78] Cao G, Chen X, Kysar JW. Thermal vibration and apparent thermal contraction of single-walled carbon nanotubes. Journal of the Mechanics and Physics of Solids. 2006,54 (6):1206-36.

[79] Che J, Cagin T, Iii WAG. Thermal conductivity of carbon nanotubes. Nanotechnology. 2000,11 (2):65-9.

[80] Prasher R. Thermal boundary resistance and thermal conductivity of multiwalled carbon nanotubes. Physical Review B. 2008,77 (7):11.

[81] DRESSELHAUS MS, EKLUND PC. Phonons in carbon nanotubes. ADVANCES IN PHYSICS. 2000,49:705 - 814.

[82] Maniwa Y, Fujiwara R, Kira H, Tou H, Kataura H, Suzuki S, et al. Thermal expansion of single-walled carbon nanotube (SWNT) bundles: X-ray diffraction studies. Physical Review B. 2001,64 (24):241402.

[83] Lim Y-S, Yee K-J, Kim J-H, Hároz EH, Shaver J, Kono J, et al. Coherent Lattice Vibrations in Single-Walled Carbon Nanotubes. Nano Letters. 2006,6 (12):2696-700.

[84] Dumée L, Wright S, Sears K, Skourtis C, Schütz J, Finn N, et al. Thermal properties of carbon nanotube macrostructures. ICONN102010.

Supplementary materials

Table 2 Main scattering dimensions found from the integrated scattering patterns – unit (Å) – the feature number corresponds to the main peaks or knees visible on the scattering patterns

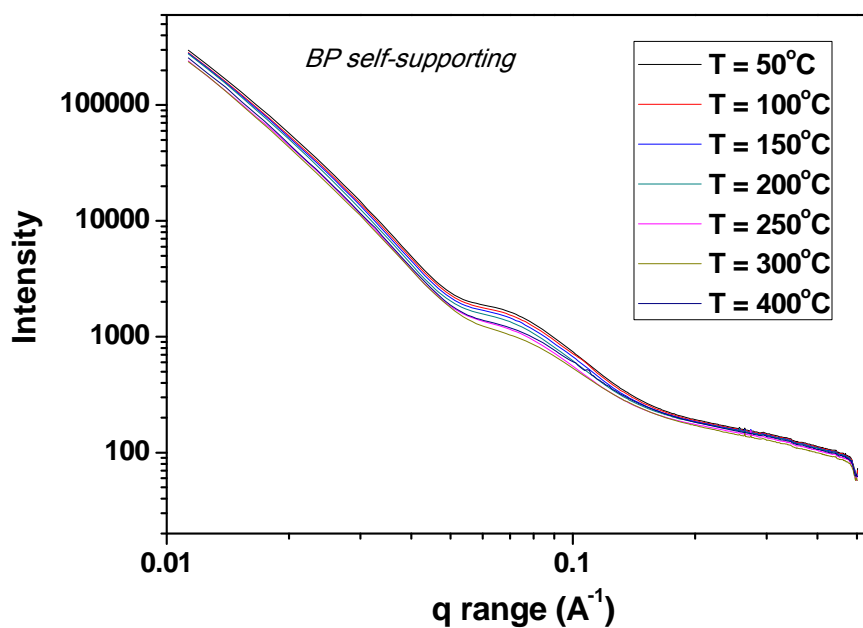|								
CNT forest	**97.4**				**21.5**	**18.3**		**14.1**
Gold coated	83.6	24.5	23.7	22.2		18.3	14.6	14.2
PS infiltrated	79.4	24.5	23.7	22.9		18.2		14.1
Acetone	76.8	24.5	23.7	22.9	21.5	18.3		14.2
Self-supporting	80.8	24.5	23.7	22.9	21.3	18.2		14.1

Figure 9 Scattering intensity of the self-supporting BP at different temperatures
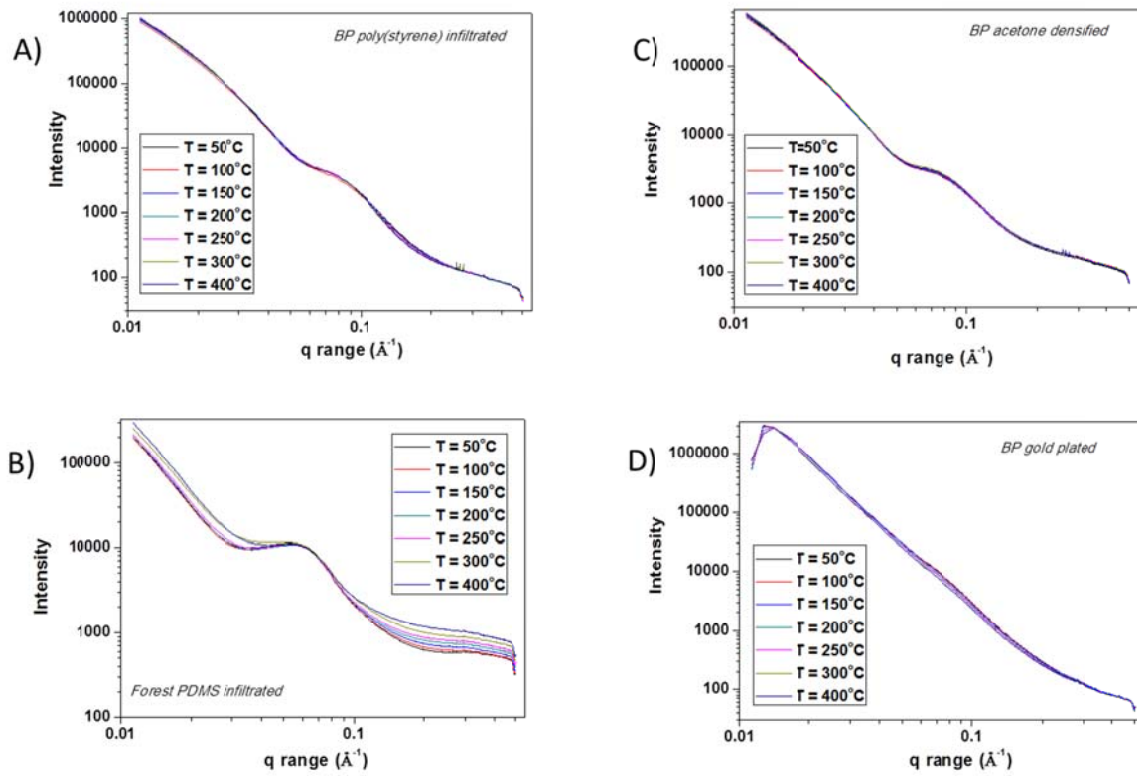
Figure 10 Scattering intensity for A) PS BP composite, B) PDMS infiltrated forest C) acetone densified BP and D) gold plated BP, at different temperatures